Computational discovery of new 2D materials using deep learning generative models

Yuqi Song, Edirisuriya M. Dilanga Siriwardane, Yong Zhao, and Jianjun Hu *

Department of Computer Science and Engineering,

University of South Carolina,

Columbia, SC 29201

E-mail: jianjunh@cse.sc.edu

Abstract

Two dimensional (2D) materials have emerged as promising functional materials with many applications such as semiconductors and photovoltaics because of their unique optoelectronic properties. While several thousand 2D materials have been screened in existing materials databases, discovering new 2D materials remains to be challenging. Herein we propose a deep learning generative model for composition generation combined with random forest based 2D materials classifier to discover new hypothetical 2D materials. Furthermore, a template based element substitution structure prediction approach is developed to predict the crystal structures of a subset of the newly predicted hypothetical formulas, which allows us to confirm their structure stability using DFT calculations. So far, we have discovered 267,489 new potential 2D materials compositions, where 1,485 probability scores are more then 0.95. Among them, we have predicted 101 crystal structures and confirmed 92 2D/layered materials by DFT formation energy calculation. Our results show that generative machine learning models provide an effective way to explore the vast chemical design space for new 2D materials discovery.

Keywords

2D materials, generative adversarial network, random forest, template based substitution, DFT calculation, layered materials

1 Introduction

Two dimensional materials such as graphene and hexagonal boron nitride have the potential to create new electronics and technologies such as spintronics, catalysis, and membranes owing to their exotic vibrational, electronic, optical, magnetic, and topological behaviors. ²⁻⁵ Using density functional theory (DFT) based screening, Mounet et al.⁶ have found 1,825 compounds with requisite geometric and bonding criteria that should make them relatively easy to exfoliate and so produce novel 2D materials with potentially interesting physical and electromagnetic properties. They discovered 56 ferromagnetic and antiferromagnetic systems, including half-metals and half-semiconductors. This greatly expands the list of predicted 2D materials and could fill the gaps in the characteristics and properties of the likes of graphene, phosphorene, and silicene. Zhou et al. proposed a high-throughput computational materials design framework, which screened 5,000 compounds from the Materials Project Database (MP), and found 205 layered materials for water splitting photocatalysts and validated 36 kinds of 2D monolayers stability. One can also expand the list of 2D materials by chemical substitutions, alternative site decorations, crystal structure prediction and so on. 8 Several screening approaches have been proposed to find 2D materials from known layered bulk materials. 9 A simple criterion of comparing experimental lattice constants and lattice constants mainly obtained from Materials-Project DFT calculation repository is used to find potential 2D materials: 9 a relative difference between the two lattice constants for a specific material is greater than or equal to 5% is used to identify good candidates for 2D materials. Haastrup et al. ¹⁰ developed the Computational 2D Materials Database (C2DB), which contains a variety of structural, thermodynamic, elastic, electronic, magnetic, and optical properties of around 1500 2D materials distributed over more than 30 different crystal structures. More recently, Zhou et al. ¹¹ developed 2DMatPedia, an open computational database of 6351 two-dimensional materials by screening all bulk materials in the database of Materials Project for layered structures by a topology-based algorithm and theoretically exfoliating them into monolayers. New 2D materials have also been generated by chemical substitution of elements in known 2D materials by others from the same group in the periodic table. These databases of experimental or hypothetical 2D materials have made it possible for discovering novel function materials. ^{12–16}

Despite these efforts, the scale of experimental and hypothetical 2D materials is still limited because of long experimental period and high cost. ¹⁷ For example, computational generation of novel new materials have been proposed in the name of inverse materials design, ¹⁸ in which new materials are to be searched to achieve a given specific function, most of these methods involve a global optimization or search/sampling procedure to explore the search space. ¹⁹ However, most of such inverse design research is based on screening known materials. Suleyman Er et al. ²⁰ proposed an elemental substitution based approach and applied it to known 2D materials structural prototypes to generate a large number of hypothetical 2D materials, and then filtered those materials based on several criteria. They deposited their predicted 2D materials in their V2DB database.

To expand the scope of 2D materials, we propose to design a generative deep learning method to discover novel 2D materials in uncharted composition space. Our approach is based on a high-accuracy composition based 2D materials classifier, which is used to screen millions of hypothetical materials compositions generated using our MatGAN, a generative adversarial network (GAN) based model²¹ that learns to generate chemically valid hypothetical materials. Based on 2.65 million generated samples, we have identified 267,489 hypothetical 2D materials. Furthermore, we use element substitute method to predicted the crystal structures, and then confirm their structure stability using DFT calculations.

Our contributions can be summarized as follows:

- We propose a composition based 2D materials classifier model which achieves high prediction accuracy when trained with known 2D materials.
- We combine the 2D materials classifier and the composition based generative machine learning to discover new 2D materials, which greatly expand the space of 2D materials.
- We apply a template based element substitution based structure prediction approach
 to get the structures of hypothetical 2D materials and verify them using DFT formation energy calculations, exfoliation energy calculation and phonon thermostability
 verification.

2 Materials and Methods

2.1 2D materials discovery framework

The schematic diagram of our 2D materials discovery framework includes the following four modules (Figure 1): a GAN based hypothetical materials generator, a composition based 2D materials classifier, a template based structure predictor, and a DFT confirmation procedure. The hypothetical materials generator is trained with known inorganic materials in the Materials Project database to learn the composition rules of forming stable chemically valid materials compositions. Then, we use the generative module to breed a large number of hypothetical formulas (two million in our study). These formulas are then subjected to chemical validity tests including charge neutrality check and electronegativity check. After that, the remaining samples will be screened by the 2D materials classifier using composition alone. To verify the predicted 2D materials compositions, we apply template based element substitution to generate their hypothetical structures for a subset of 624 predicted 2D materials compositions. Using DFT calculations, the stability of these structures is calculated to verify

the existence of these candidate 2D materials from which we identified twelve potentially stable materials.

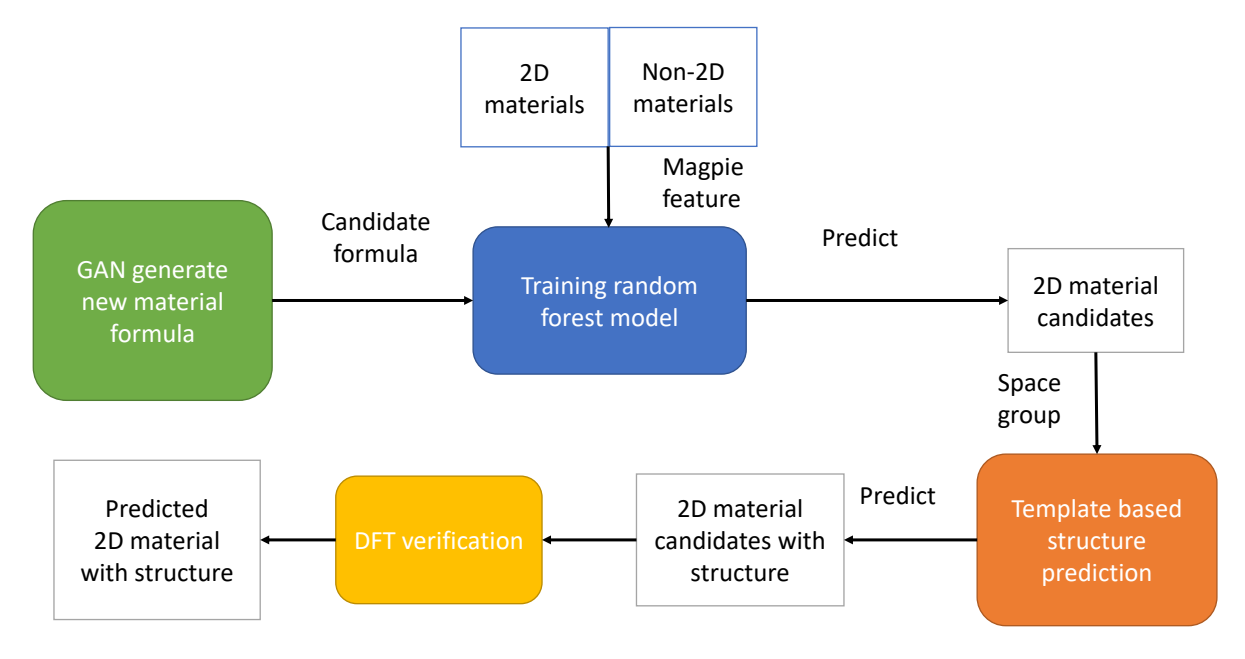


Figure 1: Framework for generation and prediction of 2D materials. It comprises four components. The green part: a GAN based composition generation module for breeding chemically valid materials. The blue part: a composition based random forest 2D materials classifier. The orange part: a template based element substitution structure predictor, as well as yellow part: DFT validation.

2.2 Generative deep learning for hypothetical inorganic materials

In the material design research area, one core task is to explore chemical space for searching new materials. In our previous work, a generative machine learning model (MatGAN)²¹ is designed to efficiently generate new hypothetical inorganic materials composition based on generative adversarial network (GAN).²² There are two main tasks of MatGAN: one is how to suitably represent material composition; the other one is how to design the generative adversarial network for generating new materials.

When exploring the representation of inorganic materials, we found that there totally are 85 elements in ICSD dataset; and there are no more than 8 atoms per element in any specific compound. Therefore, each material could be represented as a sparse matrix M of dimension

 8×85 with 0/1 cell values, where $M_{i,j} = 1$ means the number of atoms of the element at column j is i + 1. Figure 2 shows the encoding matrix for $PuP_2H_6CO_8$.

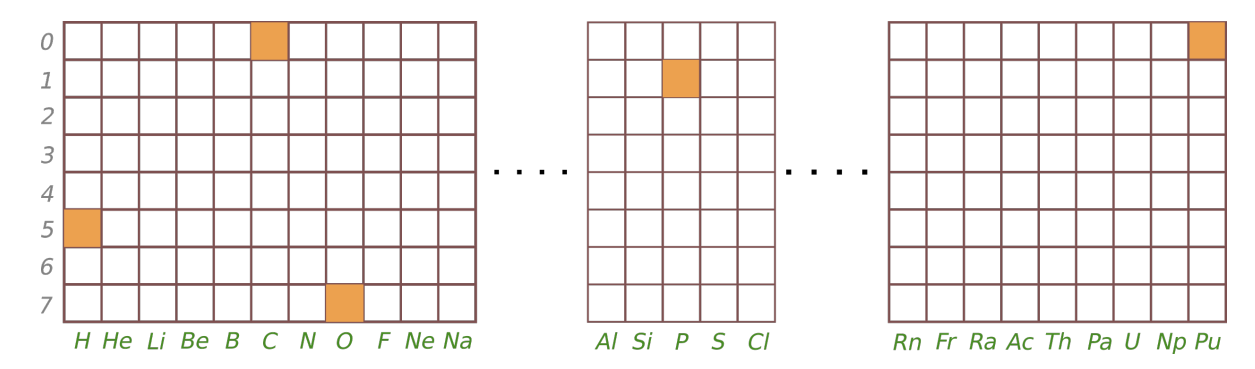


Figure 2: One hot representation of material composition PuP₂H₆CO₈. Brown color indicates the atom number of corresponding element in the specific material.

The architecture of MatGAN is shown in Figure 3. In this generative adversarial network training, a generator is trained from existing real material representations to generate new samples. Meanwhile, the discriminator tries to differentiate real samples from generated samples; as the feedback, the discrimination loss is then used to guide the training of the generator and the discriminator's parameters to reduce this difference. These two training processes are repeated until good performances of both the generator and the discriminator are achieved. In order to avoid the gradient vanishing issue of standard GAN, we adopt the Wasserstein GAN, ²³ which replaces the JS divergence distance with the Wasserstein distance. The generator loss and discriminator loss are defined in the following equations:

$$Loss_G = -E_{x:P_q}[f_w(x)] \tag{1}$$

$$Loss_D = E_{x:P_q}[f_w(x)] - E_{x:P_r}[f_w(x)]$$
 (2)

where, P_g and P_r are the distributions of generated materials and real materials; $f_w(x)$ is the discriminant network. Equation (1) and (2) are used to guide the training process. The smaller the $Loss_D$, the smaller the Wasserstein distance between the generated samples and the real samples and the better the GAN is trained. We have generated 2,650,623 hypothetical materials compositions, and 1,940,209 of them satisfy both charge neutrality and electronegativity balance criteria via Semiconducting Materials from Analogy and Chemical Theory (SMACT)²⁴ tool. The charge neutrality check means that the total charge in a compound should be 0, namely $\sum_i Q_i n_i = 0$, where i are the elements in the compound and Q are the charges. Electronegativity is often used in high-throughput screening, Ginley²⁵ presented how the simple geometric mean of the electronegativities of a compound, SMACT tool has a built in function to calculate this property for a given composition.

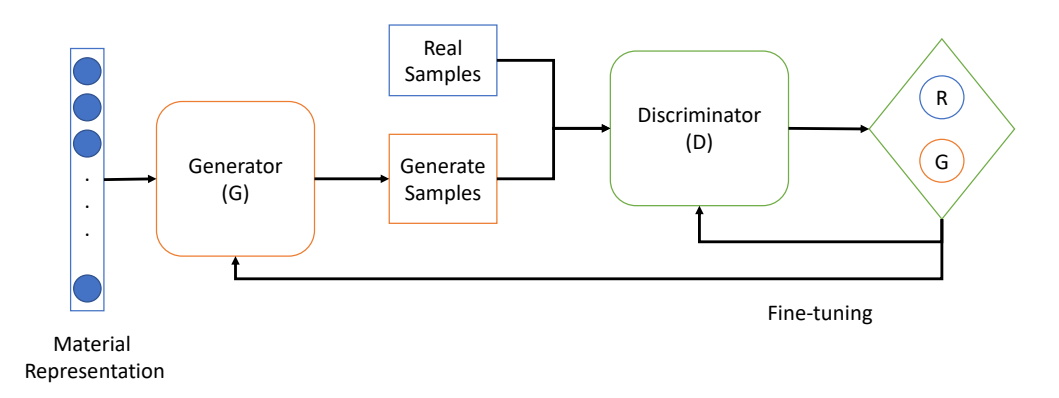


Figure 3: Architecture of MatGAN. Generator (G) learns from known material compositions to generate realistic samples while discriminator (D) learns to determine whether a sample is a real one or generated one. Alternative training of D and G will improve the performance of both G and D.

2.3 Composition based classifiers for predicting 2D materials

Predicting whether a material is 2D structure can be regarded as a binary classification problem. Our goal is to screen unknown 2D materials from MatGAN-generated materials by training a random forest classifier with verified 2D and non-2D materials, and then predicting the probability of being a 2D material of each new material.

Specifically, we employ the Random Forest $(RF)^{26}$ as the surrogate model for predicting the 2D probability given a material' Magpie composition features. Magpie feature set 27 is a well-known descriptor set for composition based machine learning models, those features

are calculated by the matminer library²⁸ which is a Python-based platform that facilitates data-driven methods for analyzing and predicting material properties by calculating a variety of descriptors from material compositions or crystal structures. Basically, magpie feature set calculate the mean, mean absolute deviation, range, minimum, maximum and mode for 22 different elemental properties for all the elements contained in a formula (132 features in total). This elemental property category includes attributes such as the maximum row on periodic table, average atomic number and the range of atomic radii between all elements present in the material. Those 132 features of each material will be calculated and used in our random forest model training.

RF is a supervised bagging ensemble learning algorithm. The idea behind random forests is to exploit the wisdom of the group. RF builds many decision trees in a random way with low correlation among them. After building the forest, when a new sample needs to be classified, each decision tree makes a judgment separately to vote which category the sample belongs to. Random forest improves the prediction accuracy without significantly increasing the amount of computation, and it is relatively robust to unbalanced data.

In the data preparation stage, we first collect known 2D and non-2D materials, as well as MatGAN generated new materials. Then, we calculate the Magpie features for all of them. In training the random forest model, known 2D materials and non-2D materials are treated as positive and negative samples to train the RF classifier with 10-fold cross-validation. The RF hyper-parameters are tuned to achieve good prediction performance with detailed settings explained in Section 3.2.2. Afterward, the trained RF model is utilized to predict the labels and probability scores of 2D for generated hypothetical new materials.

2.4 Template based structure prediction

Although we have predicted the 2D probability scores of the hypothetical new materials generated by our MATGAN algorithm and the candidates with their probability scores greater than 95% are likely to be 2D materials, it is not enough to verify their existence by DFT

calculation of their formation energy or phonon calculation based stability check. However, crystal structure prediction of complex compositions using current ab initio crystal structure prediction algorithms are not feasible.²⁹ To address this issue, we propose to use the template based or element substitution based structure prediction method, which is shown in Figure 4.

Firstly, for each predicted 2D formula, we use the Crystal Structure Prediction Network (CRYSPNet)³⁰ tool to predict its space group that the formula most likely belongs to. This method consists of many neural network models to predict the material's space group, Bravais lattice, and lattice constants. As CRYSPNet only needs chemical composition information as input, we use it to estimate the top 3 potential space groups for each new hypothetical 2D material.

Next, we try to find similar template materials from known 2D materials in the 2dMatpedia database. Specifically, For each new 2D formula with three potential space groups, we search the target 2D material that has the same number of elements and the same space group. However, one formula may lead to many potential target 2D material template. To identify the most similar template material, we use Element Movers Distance (ElMD)³¹ machine learning model to calculate and sort similarities between the candidate materials and potential template materials. ElMD is a similarity measure for chemical compositions, which is measured Earth Mover's Distance (EMD)³² between two compositions from the ratio of each of the elements and the absolute distance between the elements on the modified Pettifor scale.

Finally, we select the top 10 most similar known 2D materials as the structure templates according to the ElMD values. New 2D material's structures could be then predicted by one to one element substitution from those pairs. For example, as shown in Figure 4, the structure of XY is predicted from the structure of AB by using X to replace A (gray atom) and Y to replace B (yellow atom).

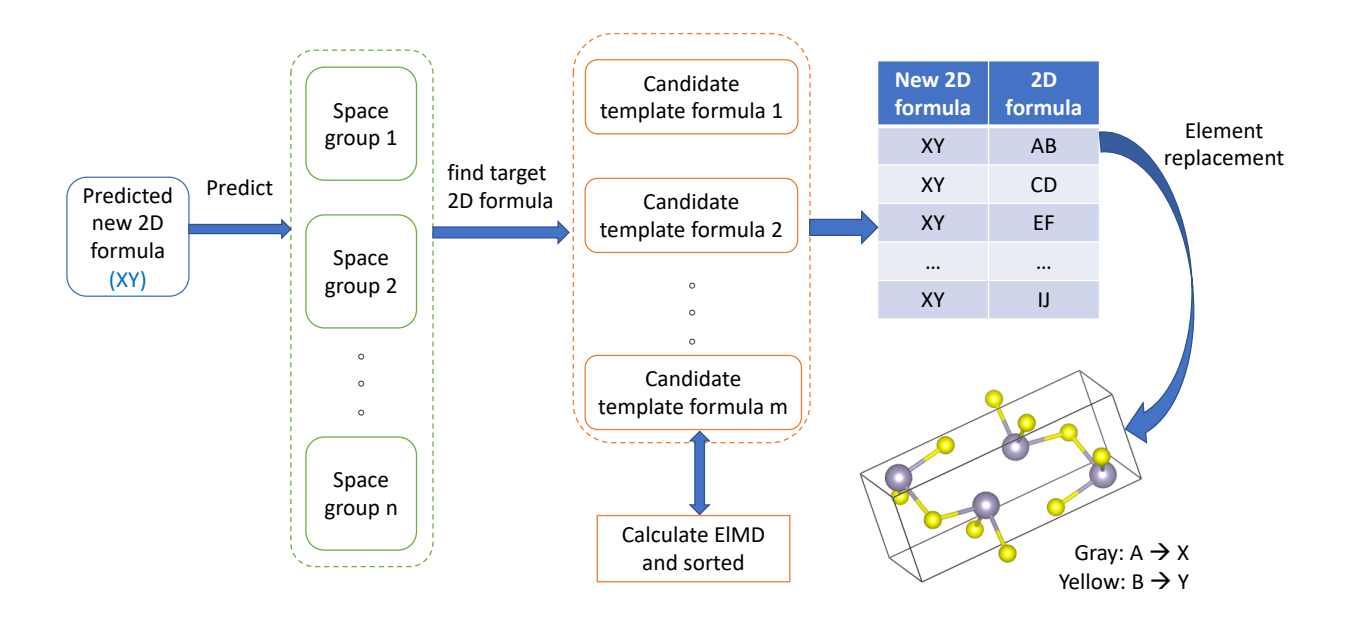


Figure 4: The framework of template based structure prediction. The main parts are: predicting new formula's space group; finding candidate template formulas according to the same element number and the same space group; calculating and sorting ElMD between the new formula and template formulas; selecting top n templates to do element substitution to get the new formula's structure.

2.5 DFT calculation for verification

The density functional theory (DFT) calculations were performed based on the Vienna ab initio simulation package (VASP). ^{33–36} The electron-ion interactions were considered by using the projected augmented wave (PAW) method. ^{37,38} The energy cutoff value was set as 500 eV. The generalized gradient approximation (GGA) based on the Perdew-Burke-Ernzerhof (PBE) pseudopotentials ^{39,40} represented the exchange-correlation potentials. The energy convergence criterion was set as 10^{-7} eV, while the force convergence criterion of the ionic steps was considered as 10^{-2} eV/Å. The Γ -centered Monkhorst-Pack k-meshes were considered to perform the Brillouin zone integration for the unit cells. The van der Waals interactions were considered using DFT+D3 with Becke-Jonson damping. ^{41,42} Formation energy per atom (E_{form}) of a material were calculated based on Eq.3. Here, E[Layered] is the total energy per

unit formula of the corresponding material, $E[A_i]$ is the energy of i^{th} element of the material, x_i represents the number of atoms of i^{th} element in a unit formula, and N indicates the total number of atoms in a unit formula of the material (e.i., $N=\sum_i x_i$). Exfoliation energies were determined using Eq. 4. In this equation, E[Monolayer] is the total energy per unit formula of the monolayer exfoliated from a 2D layered material. S is the area of the layered material's surface, which is perpendicular to out-of-plane direction of the monolayer.

$$E_{\text{form}} = \frac{1}{N} (E[\text{Layered}] - x_i \sum_{i} E[A_i])$$
 (3)

$$E_{\text{exf}} = \frac{-1}{2S} (E[\text{Layered}] - E[\text{Monolayer}]) \tag{4}$$

3 Experiments

3.1 2D materials Dataset

All the 2D materials are collected from 2DMatPedia, ¹¹ an open computational database of two-dimensional materials, which is constructed by a topology based screening algorithm and element substitutions. There are 6,351 2D materials in total, they are regarded as positive training samples in our work. We also collect all existing materials from the materials project database with 126,356 materials in total. After removing known 2D materials, there are 115,498 negative samples. We use the MatGAN model to generate 2,650,264 new materials as candidates for 2D materials prediction.

Table 1: Datasets

Dataset	Amount	Role		
2dMaterials	6,351	positive training sample		
MaterialProject	$126,\!356$	negative training sample (exclude 2D materials)		
$ICSD_2M$	2,650,624	potential new material		
V2DB	294,077	comparative dataset		

3.2 Results

3.2.1 Generation of candidate inorganic materials

Trained with 291,840 inorganic materials compositions in Material Project database, a generative deep learning model (MATGAN) is used to generate 2,650,623 new compositions, and then charge neutrality and balanced electronegativity are used to screen out 1,947,792 formulas, among which 1,940,209 are not in the training set.

The number of generated 2-element materials, 3-element, 4-element, ≥5-element are 1217, 18946, 36827, 78639, respectively. There are two reasons to explain why binary materials account for the least proportion: one is the diversity of the combination of two elements is much less than that of five elements. The other is many binary materials have already been discovered. The generated 2-element materials play an important role in subsequent research because most known 2D materials are binary materials.

In order to better display the generated materials distribution information, we draw a line chart (as shown in Figure 5) to show the frequencies of 112 elements ordered by atomic number in three datasets: generated ICSD-2M candidate materials by MatGAN, the published 2D material dataset and the predicted 2D materials. From these three curves, we can see that the top 5 crests positions basically overlap, the number ranges are 7-9, 15-17, 32-35, 50-53, and 80-83. It proves that the space of candidate materials generated by MatGAN is consistent with the real 2D materials. Furthermore, it provides a solid candidate range for the following 2D new material prediction.

3.2.2 Performance of the 2D materials classifier

The hyper-parameter configuration for training 2D random forest classifier is set as follows: we set the maximum tree depth (max_depth) to be 20 and the number of decision trees $(n_estimators)$ as 250. There are 6351 2D material samples and 15,959 non-2D samples. In order to mitigate the imbalanced positive and negative samples, we randomly select 1.5 times

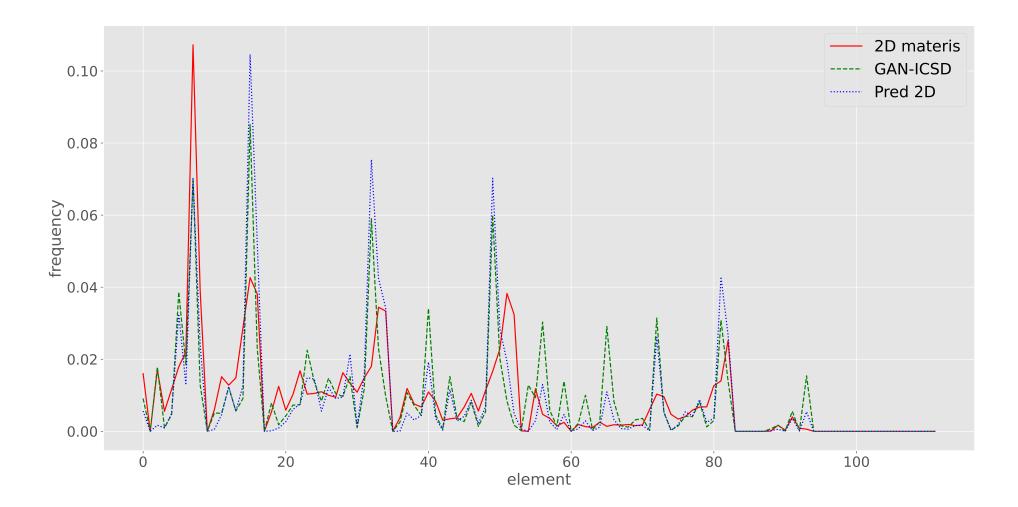


Figure 5: Element frequency distribution. The abscissa represents 112 chemical elements arranged according to the atomic number from hydrogen (H) to Copernicium (Cn), vertical axis indicates the frequency of each element. The red curve denotes the distribution information of 2dMaterials dataset. The green curve shows our generated candidate materials. The blue line represents our predicted 2D materials.

the number of positive samples as negative samples. Besides, the class weight parameter is set to be balanced. With these settings tuned per feature iteration, we train the RF 2D materials prediction models and evaluate their performance. Our algorithm is implemented using the Scikit-Learn library in Python 3.6.

To evaluate the prediction performance of our model, precision, recall, accuracy, F1 score, and receiver operating characteristic area under the curve ROC are used as performance metrics. ROC is plotted with TPR and FPR as the vertical and horizontal axes under different threshold settings.

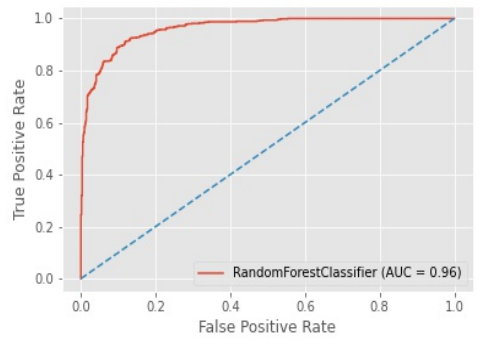
$$TPR = \frac{TP}{TP + FN} \tag{5}$$

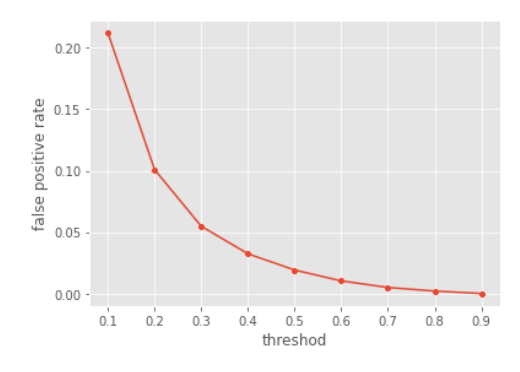
$$FPR = \frac{FP}{FP + TN} \tag{6}$$

The accuracy, precision, recall, and F1-measure of the RF classifier with 10 fold cross-

validation is 88.97%, 88.98%, 88.96%, and 88.96%. Figure 6(a) shows the ROC curve of the classifier with an AUC score reaching 96%.

We also use a series of thresholds to differentiate 2D and non-2D materials to evaluate the performance of the RF classifier, as shown in Figure 6(b). The abscissa represents the the predicted probability threshold to declare a 2D materials when its probability is higher than this threshold value; the y coordinate indicates the corresponding false-positive rate. As the threshold increases, the higher the probability score is required to be judged as a 2D material leading to lower false-positive rate.





- (a) ROC curve of our RF classifier
- (b) False-positive curve of our RF classifier.

Figure 6: performance of random forest classifier. (a) shows the performance of the trained 2D materials Random Forest classifier by ROC curve and AUC score; (b) shows the false-positive rates of the trained 2D materials Random Forest classifier with different thresholds

3.2.3 Finding new 2D materials using our framework

To identify interesting hypothetical new 2D materials, we applied our RF-based 2D materials classifiation model to screen the 2.6 million hypothetical materials generated by our Generative Adversarial Network (GAN) based on new materials composition generator. ²¹ After predicting the probability of each candidate belonging to 2D materials, we sort them by the probability scores. The statistics of the predicted 2D materials with different probability thresholds are shown in Table 2. With a stringent probability threshold of 0.95, our algorithm has identified 1,485 hypothetical 2D material formulas with 266 binary, 361 ternary, 327 quartenary

candidates. When the threshold is lowered to 0.9, the number of candidate 2D formulas increases to 5,034 or to 18,451 with threshold of 0.8.

To demonstrate how the newly predicted 2D materials are distributed in the composition space, we apply t-sne dimension reduction tool⁴³ to map the normalized Magpie features of the 6351 2D materials in the 2D materials and the predicted 2D materials, and then plot their distribution in Figure 7. In Figure 7(a), We apply the same dimension reduction transformation to both the training set and the newly predicted 2D materials and visualize their distribution where red points are training samples, and blue points are the 1485 predicted 2D materials with the highest probability scores. Similarly, top 20,0000 predicted 2D materials are drawn as blue points in Figure 7(b) together with known 2D materials used for training. We found that in Figure 7(a) the majority of blue points are located in the dense red point areas in the bottom left corner (which can be seen also from Figure 7(c)), indicating that our predicted 2D materials have similar composition distribution with regard to known 2D materials. Figure 7(b) further confirms this composition distribution match, in which we find that the blue points in general only appear in areas with red points. The areas with sparse red points also contain few blue points. Figure 7(c) shows the distribution of 20,000 hypothetical 2D materials in the V2DB dataset against the known 2D materials. It is found these candidate 2D materials have different composition distribution as regard to the known 2D materials: many yellow points appear in areas without red points. Quite many yellow points reach out of the boundary defined by the red points. For better comparison, top 6000 predicted samples by our method and the V2DB are drawn in Figure 7(d) together with 6351 known 2D materials. It can be seen that the majority of the overlapped blue and yellow points (117 as shown in Table 3) are located in the lower-left corner, which means there are new 2D materials that are jointly predicted by both methods.

To screen out top candidate materials, we use the Roost algorithm ⁴⁴ for formation energy prediction, which is a graph network based machine learning model for materials property prediction using only composition information. After predicting the formation energies of

all candidates, we draw a histogram of formation energy distribution, as shown in Figure 5. Furthermore, we filter out those with probability scores greater than 0.95 and then sort them by the formation energy in ascending order and pick the top 40 candidates with 2, 3, and 4 elements respectively. The results are in Table 4.

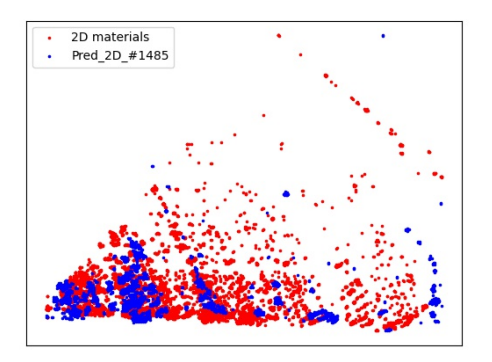
Furthermore, we analyze the 2DMatPedia dataset, 2-element materials occupy 65%, 3-element materials, and 4-element materials account for 25% and 9%, therefore, from the perspective of the probability distribution, our prediction is meaningful. We also find that the predicted 2D probabilities of 2-element materials are in general higher than those of 3-element materials and 4-element materials, corresponding to the fact that the majority of known 2D materials (65%) are binary materials. We also count the number of our predicted new 2D materials with 2D probability greater than 0.5 that overlap with those in V2DB and 117 hypothetical 2D materials are found to be predicted by both methods. Table 3 shows the overlapped candidate 2D materials in five parts according to their 2D probability scores. It is found the overlapped materials with 2D probability greater than 0.8 account for nearly 50% of all overlapped candidates.

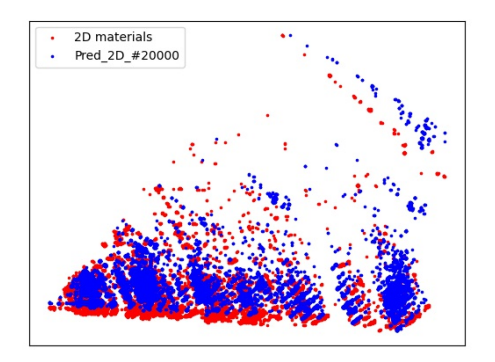
Table 2: Statistics of predicted 2D materials

2D Prob	# of Predicted 2D formula	# 2 element	# 3 element	# 4 element	$\# \geq 5$ element
0.95	1,485	266	861	327	31
0.9	5,034	439	2,617	1,695	283
0.8	18,451	729	8,123	7,316	2,283
0.7	$48,\!592$	942	16,827	21,430	9,393
0.6	119,489	1,146	28,172	51,998	38,173
0.5	267,489	1,340	$40,\!382$	99,943	125,824

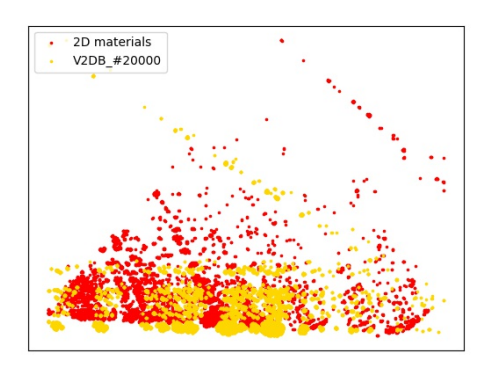
3.2.4 Structure prediction and verification

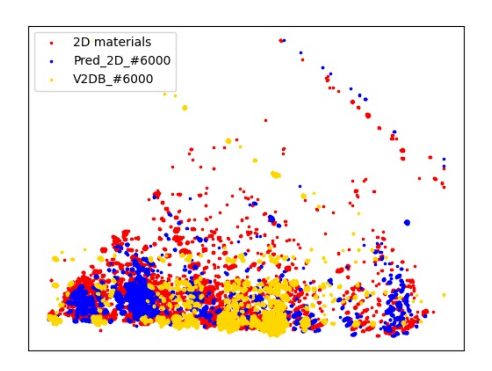
To verify the predicted 2D materials, we pick 1485 predicted material formulas with the highest probability scores (≥ 0.95) and use the template based structure prediction method to find their structures. With the result that we find 101 materials' templates of known layered materials or 2D materials in the 2DMatPedia database. We then predict the space





(a) New 2D materials (Probability > 0.95) vs.(b) 20,000 2D materials in the whole MP comknown ones position space





(c) 20,000 2D materials in the V2DB

(d) 6,000 2D materials in MP and V2DB vs. known ones

Figure 7: Distribution of the new and old 2D materials using t-sne visualization. Red ones are known 2D materials, blue ones are our predicted 2D materials while yellow ones are predicted 2D materials from V2DB. Figure (a) shows 1485 points with the highest 2D probability scores. (b) and (c) display distribution of 20,000 predicted samples from our model and from V2DB respectively. For better visual comparison, 6,000 predicted 2D materials from our model and from V2DB are shown together in (d).

Table 3: Predicted hypothetical 2D materials that overlap with V2DB $\,$

Formula	Prob	Formula	Prob	Formula	Prob	Formula	Prob	Formula	Prob
	> 0.9		> 0.8		> 0.7		> 0.6		> 0.5
AgS	0.9999	ZrClS	0.8997	TiSeCl	0.7913	VISe	0.6879	NiF	0.5998
AlS	0.9982	AlIS	0.8926	ZrSeF	0.7900	NiSeCl	0.6830	ZrTeN	0.5993
ScI	0.9840	VClF	0.8917	SbSeO	0.7856	CoBrF	0.6797	MnSeS	0.5872
InTeS	0.9753	FeClS	0.8909	ZrTeSe	0.7802	NiSF	0.6794	SrSF	0.5840
SnTeSe	0.9748	PbTeS	0.8884	MnBr	0.7793	RhSeS	0.6759	YSeS	0.5709
SnTeS	0.9737	GeSF	0.8852	MnIS	0.7782	CoTeS	0.6740	NbSeO	0.5669
PbTeSe	0.9465	BiSF	0.8830	CuTeO	0.7647	CrSeO	0.6732	CoF	0.5638
SbSeF	0.9421	TiClF	0.8800	CoCl	0.7602	CoSF	0.6714	NbTeO	0.5636
SbClS	0.9418	ZnBrS	0.8777	GeSO	0.7588	RhTeS	0.6710	TaSO	0.5604
GeClS	0.9409	MnClS	0.8757	ZnSF	0.7579	MnBrN	0.6697	TaTeS	0.5506
AsClS	0.9374	SnSeO	0.8727	ZnSO	0.7579	AlSeO	0.6609	NiSO	0.5474
SbSF	0.9224	ZnClS	0.8725	AgSO	0.7557	PbTeO	0.6540	NiSeO	0.5419
NbSe	0.9221	AgIS	0.8670	CuSeF	0.7546	MnSeO	0.6473	YTeS	0.5249
AlSeS	0.9197	PbSeO	0.8535	MnSF	0.7518	VSeS	0.6451	TiSeN	0.5186
SnSO	0.9181	AsSF	0.8532	MnSeF	0.7466	NbSeF	0.6367	SrClS	0.5120
BiTeS	0.9102	AgTeS	0.8524	AsSO	0.7422	RuTeS	0.6310		
AlTeS	0.9060	PbSO	0.8494	AgSeO	0.7406	TaSeO	0.6217		
		YClS	0.8471	ZrSeS	0.7392	FeSeF	0.6190		
		BiTeF	0.8462	CoClF	0.7362	TaTeSe	0.6077		
		NiClS	0.8457	PdFO	0.7319	CrTeO	0.6066		
		YTeF	0.8457	ZrTeO	0.7317	ZrSeN	0.6014		
		CoClS	0.8433	MnI	0.7312				
		VClS	0.8397	CuSF	0.7245				
		VSF	0.8395	AlSO	0.7239				
		AlTeCl	0.8285	TiTeS	0.7230				
		NiBr	0.8254	NiClO	0.7077				
		SbSeS	0.8220	NiTeCl	0.7056				
		AgSeS	0.8217	NbSO	0.7005				
		BiSO	0.8201						
		ZnClF	0.8176						
		TiSeF	0.8155						
		MnCl	0.8077						
		FeI	0.8074						
		AlSeF	0.8017						
		AlTeF	0.8015						
		CoI	0.8002						

Table 4: Hypothetical 2D materials sorted by predicted formation energy (only top 120 are listed here) $\,$

2 Elements			3 Ele	ments	4 Elements			
Formula	Prob	$E_{form}[Layered-ML]$ (eV/atom)	Formula	Prob	$E_{form}[Layered-ML]$ (eV/atom)	Formula	Prob	$E_{form}[Layered-ML]$ (eV/atom)
ZrF3	0.9876	-3.8661	ScYF3	0.9760	-3.3429	NbMoCl5S2	0.9757	-1.5188
YF2	0.9880	-3.7549	NbMoF6	0.9720	-3.0069	CrNbMoCl8	0.9638	-1.4547
TaF4	0.9990	-3.4457	ZnTaF5	0.9755	-2.9848	CrNbRuCl8	0.9598	-1.3912
SiF3	0.9607	-3.3363	NbRuF7	0.9665	-2.7521	NbRuCl5S2	0.9753	-1.3857
ZrF2	0.9997	-3.1413	InSnF5	0.9519	-2.7437	NbRuCl4S2	0.9712	-1.3826
ScF	0.9760	-2.7647	TaIrF7	0.9794	-2.7379	NbRuCl6S	0.9673	-1.3719
YF	0.9640	-2.747	NbRuF6	0.9708	-2.7165	NbRuCl6S2	0.9633	-1.3688
GeF3	0.9705	-2.6997	TaWO5	0.9732	-2.6845	CrMoCl5S	0.9517	-1.3163
NbF2	0.9671	-2.5717	ScYCl6	0.9677	-2.6222	NbMoRuCl6	0.9676	-1.2988
YCl2	0.9919	-2.4657	NbMoO5	0.9816	-2.6101	Ga3AsCl6S2	0.9514	-1.2548
ZrF	0.9720	-2.4356	TaWF5	0.9760	-2.5844	InSn3SeCl6	0.9513	-1.2127
WF3	0.9999	-2.4182	TaIrF5	0.9511	-2.5832	SnSbAsCl8	0.9593	-1.205
TaF2	0.9880	-2.4126	ScYCl4	0.9679	-2.527	MoRuCl5S2	0.9633	-1.171
AlF	0.9999	-2.4107	YZrCl6	0.9598	-2.4481	Sn2AsCl6S	0.9550	-1.1705
ScCl2	0.9799	-2.338	ScZrCl6	0.9518	-2.3783	InSn3Cl4S2	0.9907	-1.1704
GaF	0.9995	-2.0765	MoRuF6	0.9708	-2.352	MoRuCl6S2	0.9633	-1.1499
FB	0.9880	-2.0746	TaOsF5	0.9640	-2.3308	Sb2BrAsCl8	0.9671	-1.1406
F3C	0.9800	-2.0634	ScTiCl4	0.9600	-2.2386	InSnCl2S2	0.9745	-1.1381
InF	0.9880	-1.9397	VTc2F7	0.9661	-2.2366	InSnCl4S2	0.9709	-1.1229
Tc2O5	0.9650	-1.9029	VZrCl6	0.9560	-1.9388	SnSbAsCl4	0.9514	-1.1043
ErBr3	0.9674	-1.8561	YLaBr6	0.9547	-1.9262	Sn2AsCl4S	0.9628	-1.0983
OsF3	0.9837	-1.7279	TbDyBr6	0.9729	-1.8741	Sn2AsCl8S2	0.9627	-1.0955
NbCl3	0.9959	-1.7273	TiVCl6	0.9519	-1.8074	Sn3SeCl6S2	0.9509	-1.0928
S2O5	0.9859	-1.7237	Nb3Cl8S	0.9919	-1.7429	Sn2AsCl7S2	0.9587	-1.0901
NbCl2	0.9799	-1.7137	NbCl2S	0.9599	-1.6969	SnPb2Br2Cl2	0.9573	-1.0892
OB	0.9600	-1.7046	AlClS	0.9596	-1.6887	Sn2AsCl6S2	0.959	-1.0838
TaCl2	0.9950	-1.6658	TaRe2F6	0.9640	-1.6724	InSn2Cl2S2	0.9755	-1.0789
RuF2	0.9864	-1.5312	CrNbCl7	0.9677	-1.6054	Sn2As2Cl6S	0.9511	-1.0705
SF	0.9798	-1.4954	CrNbCl6	0.9758	-1.602	InSnClS2	0.9820	-1.0414
MnCl3	0.9997	-1.4641	CrNbCl8	0.9637	-1.5821	Sn2AsCl4S2	0.9628	-1.0387
CrCl4	0.9838	-1.4529	TiYBr6	0.9538	-1.5738	CuRuAgCl6	0.9629	-1.0133
SeF	0.9795	-1.436	SnPbCl6	0.9577	-1.5723	Sn2AsCl6S3	0.9587	-1.011
O3C2	0.992	-1.3673	VMnCl4	0.96	-1.5719	Sn2SeCl6S2	0.9509	-1.0109
GeCl3	0.9988	-1.3663	CrNbCl5	0.9598	-1.5622	Sn2SeCl5S2	0.9549	-1.0048
YS3	0.9618	-1.3661	Te2SO5	0.9508	-1.5303	AsGeCl6S	0.9590	-1.0045
V2S3	0.9661	-1.3311	InSnCl6	0.9795	-1.5166	AsGe2Cl6S2	0.9636	-0.9982
TiCl	0.9599	-1.3269	SnTlCl5	0.9507	-1.5121	Sn2As2Cl6S3	0.9547	-0.9832
HoS3	0.9755	-1.3082	TaWCl6	0.9794	-1.5067	Sn2SeCl4S2	0.9549	-0.9821
SmS3	0.9555	-1.3041	NbMoCl6	0.9839	-1.5054	Sn2AsCl6S4	0.9590	-0.977
YI2	0.9999	-1.2846	Cl6SSi2	0.9877	-1.5012	SnPb2Se2Cl2	0.9538	-0.9457

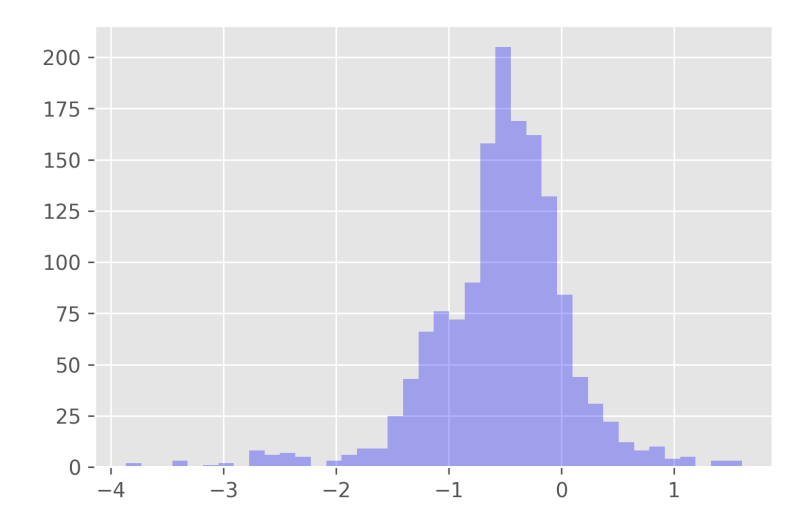


Figure 8: Formation energy distribution of predicted 2D materials.

group of our predicted 2D materials and choose the templates with the same or similar space groups. Next, element substitution method has been used to get their crystal structures. Some of the predicted 2D materials structures are shown in Figure 11. In total, 101 predicted materials with structures have been obtained.

To further verify whether these hypothetical materials are thermodynamically stable, we applied DFT first principle calculation to compute the formation energies per atom for the 101 2D-layered materials which have template structures. In total we found 92 hypothetical materials with negative formation energy (see Supplementary Table S1), there are 79 binary 2D materials, 10 ternary 2D materials and 3 quaternary 2D materials. The materials with high formation energies like TaF_4 (-2.9431 eV/atom) and SiF3(-2.1204 eV/atom) imply that the proposed method in this research is able to discover 2D layered materials which are highly thermodynamically stable against the parent compounds of their elements.

Furthermore, we studied the exfoliation possibility of 2D-layered materials using exfoliation energy based on Eq. 4. Modeling monolayers from around 100 2D-layered materials is computationally expensive. Thus, here we modeled only 31 monolayers to show that the proposed computational technique can find 2D materials with very low exfoliation energies

(see Supporting Information Table S2). The 12 materials with lowest exfoliation energies are mentioned in Table 5. The formation energies of those monolayers are also negative indicating they are stable relative to the compounds of respective elements.

In order to demonstrate that our predicted compositions and structures can be used to discover stable layered materials, we computed the elastic constants using density functional perturbation theory (DFPT) ⁴⁵ and phonon bands using Phonopy code ⁴⁶ for V₂S₃. Our DFT calculations show that V₂S₃ is a stable 2D-layered material. The structure of this material is shown in Figure 9. V₂S₃ has Triclinic crystal symmetry with P-1 (2) space group symmetry. The lattice parameters were found as a = 3.072 Å, b = 7.130 Å, c = 9.216 Å, $\alpha = 87.06$, $\beta = 80.40$, and $\gamma = 77.59$. The formation energy calculated based on Eq. 3 is around -0.618 eV/atom. The enthalpy difference between competitive phases determined based on the expression $\Delta H = E[\text{Material}] - E[\text{competitive phases}]$ using the total energy E of the material and its competitive phases. The competitive phases were found from the Material Project database. ⁴⁷ The computed maximum enthalpy difference for V₂S₃ is 0.046 eV/atom against the stable phases V₅S₈ and V₃S₄.

Based on the Hill approach, we found the Bulk modulus, Shear modulus, and Young's modulus as 26.29, 18.88, 45.69 GPa, respectively. ⁴⁸ The total energy of a material can be denoted by $E = E_0 + \frac{1}{2}V_0 \sum_{i,j=1}^6 C_{i,j} \epsilon_i \epsilon_j + O(\epsilon^3)$, when an infinitesimal strain (ϵ) is applied. Here, C is the matrix of second-order elastic constants. The Born elastic stability criteria require that the matrix be definite positive, and all eigenvalues of C and all the principal components should be positive. The relationships between the elastic constants of Born criteria of P-1 (2) crystal symmetry are very complicated since the triclinic systems have 21 independent elastic constants. ⁴⁹ Therefore, VASPKIT ⁵⁰ code was employed to calculate the elastic properties. It confirms that V_2S_3 is mechanically stable. The all phonon frequencies in Figure 10 are positive, implying the material is dynamically stable at 0 K temperature.

Moreover, we performed phonon calculations for V_2S_3 monolayer as shown in the Supporting Information Figure S1. It is clear that this nanosheet also dynamically stable at 0

K temperature. The exfoliation energy and formation energy of the monolayer are negative suggesting that V_2S_3 nanosheet can be exfoliated from the parent layered-material (see Table 5).

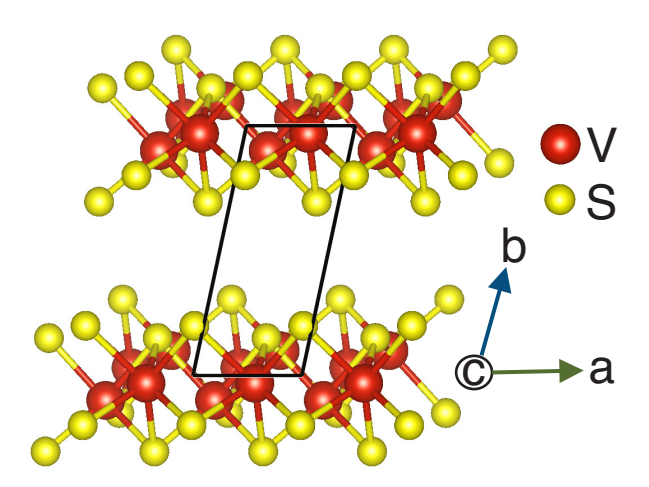


Figure 9: Structure of V_2S_3 2D-layered material

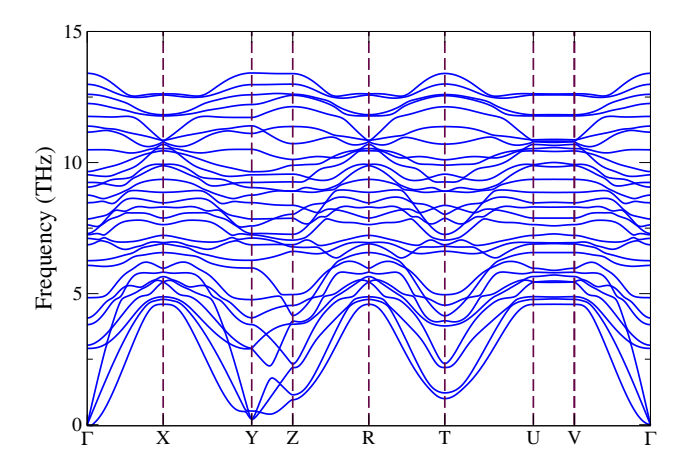
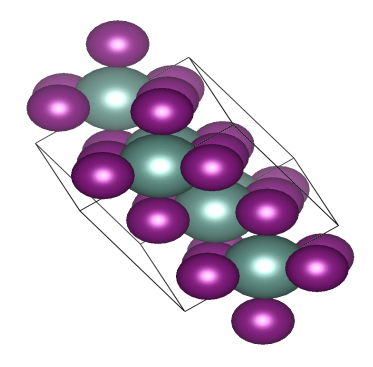
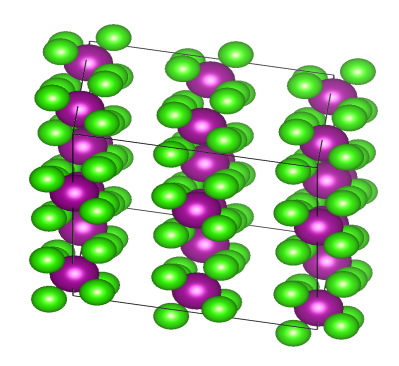


Figure 10: Phonon bands of V_2S_3 2D-layered material

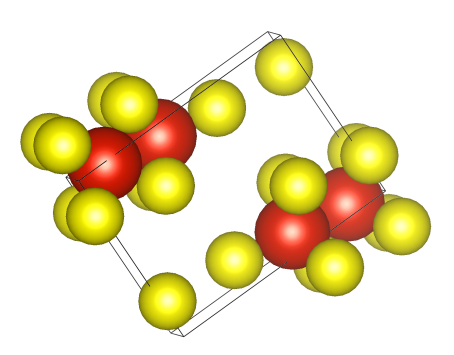
Table 5: The 12 compositions with lowest exfoliation energies found using DFT are mentioned in the table. The formation energies of layered materials using DFT ($E_{\text{form}}[\text{Layered-DFT}]$) and using the machine learning model ($E_{\text{form}}[\text{Layered-ML}]$), and the formation energies of monolayers using DFT ($E_{\text{form}}[\text{Monolayer}]$) are also stated.

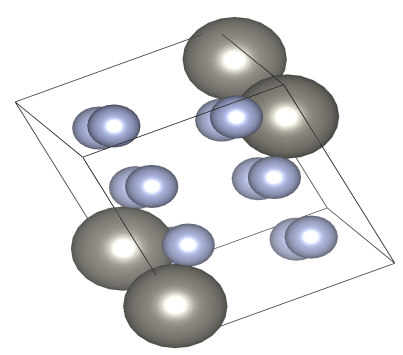
Formula	$E_{\text{form}}[\text{Layered-DFT}]$	$E_{\text{form}}[\text{Layered-ML}]$	$E_{\rm exf}$	$E_{\text{form}}[\text{Monolayer}]$
1 Ormaia			(meV)	
	(eV/atom)	(eV/atom)	(mev)	(eV/atom)
S2O5	-0.6417	-1.7237	-87.8131	-1.4659
V2S3	-0.6830	-1.3311	-11.7012	-0.8130
CoCl3	-0.2434	-1.0299	-2.4151	-1.8472
YI2	-1.1979	-1.2846	-1.1606	-1.2315
OB	-2.0188	-1.7046	-0.6184	-2.0268
TaF4	-2.9431	-3.4457	-0.1287	-2.8880
YCl2	-1.9251	-2.4657	0.5745	-3.3604
ScS3	-0.9223	-1.1463	1.6923	-0.8984
WS3	-0.2765	-0.4336	2.3043	-0.1630
SiF3	-2.1204	-3.336	2.5126	-2.0726
GaCl	-0.6627	-1.0418	2.5508	-1.6550
PBr4	-0.2054	-0.3209	2.6124	-0.0463



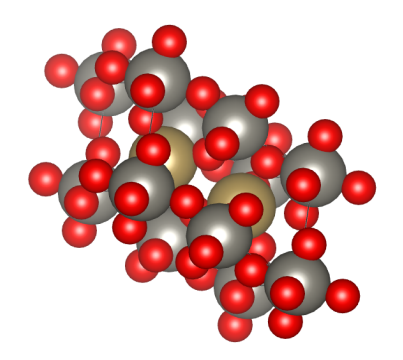


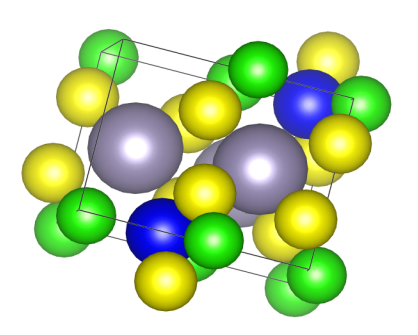
(a) 2D material YI_2 by element substitution (b) 2D materials $MnClYI_3$ by element substiwith formation energy -1.260 eV tution with formation energy -1.45 eV





(c) 2D material V_2S_3 by element substitution (d) 2D materials WF₃ by element substitution with formation energy -0.680 eV with formation energy -2.092 eV





(e) 2D material TaWO₅ by element substitu-(f) 2D materials SnAsClS₂ by element substition with formation energy -2.747 eV tution with formation energy -0.360eV

Figure 11: Selected structures of the discovered new 2D materials with DFT validation. (a) displays the predicted crystal structure for YI_2 , and its DFT calculated formation energy is -1.260 eV. The predicted crystal structures and DFT calculated formation energies for MnClYI₃ V_2S_3 , WF₃, TaWO₅, SnAsClS₂ are shown in (b),(c),(d),(e),(f), respectively.

4 Conclusion

We propose a generative inverse design approach for finding hypothetical new 2D materials. It includes a GAN based composition generation model for generating chemically valid materials formulas, a composition based random forest 2D materials classifier, a template based element substitution structure predictor, and DFT verification. Using this pipeline, we have generated 1485 hypothetical 2D material compositions with probability scores greater 95%. We computationally verified that 92 materials have negative formation energies using DFT. We also modeled 31 monolayers from the proposed structures and found that the all 31 materials provide exfoliation energies less than 200 meV showing high possibility of exfoliating nanosheets from their layered materials. These new hypothetical materials can be used to guide the screening of 2D materials for special functions using materials property prediction models. The experiments demonstrate the effectiveness of the proposed approach for discovering new 2D materials and can be used as a complement of the prototype based element substitution based generation approach. Currently, our method is constrained by the limited capability of the crystal structure prediction step, which is an unsolved problem. More powerful crystal structure prediction methods are needed to identify 2D materials of novel structural prototypes, which cannot be identified using template-based structure modeling approach as we use here.

5 Contribution

Conceptualization, J.H.; methodology, J.H., Y.S.; software, Y.S.; validation, Y.S., E.S. and J.H.; investigation, J.H., Y.S., E.S., and Y.Z.; resources, J.H.; data curation, J.H., Y.S. and Y.Z.; writing—original draft preparation, J.H. and Y.S., E.S., and Y.Z.; writing—review and editing, J.H., Y.S.; visualization, Y.S.; supervision, J.H.; funding acquisition, J.H.

Acknowledgement

Research reported in this work was supported in part by NSF under grant and 1940099 and 1905775. The views, perspective, and content do not necessarily represent the official views of the SC EPSCoR Program nor those of the NSF.

Supporting Information Available

92 Hypothetical 2D materials with DFT verified layered formation energies; the 31 compositions with exfoliation energies found using DFT calculations; phonon bands of V_2S_3 monolayer.

References

- (1) Wang, X.; Cui, Y.; Li, T.; Lei, M.; Li, J.; Wei, Z. Recent Advances in the Functional 2D Photonic and Optoelectronic Devices. *Advanced Optical Materials* **2019**, *7*, 1801274.
- (2) Gibertini, M.; Koperski, M.; Morpurgo, A.; Novoselov, K. Magnetic 2D Materials and Heterostructures. *Nature nanotechnology* **2019**, *14*, 408–419.
- (3) Akinwande, D.; Huyghebaert, C.; Wang, C.-H.; Serna, M. I.; Goossens, S.; Li, L.-J.; Wong, H.-S. P.; Koppens, F. H. Graphene and Two-dimensional Materials for Silicon Technology. *Nature* **2019**, *573*, 507–518.
- (4) Ahn, E. C. 2D Materials for Spintronic Devices. npj 2D Materials and Applications **2020**, 4, 1–14.
- (5) Zhang, X.; Chen, A.; Zhou, Z. High-throughput Computational Screening of Layered and Two-dimensional Materials. Wiley Interdisciplinary Reviews: Computational Molecular Science 2019, 9, e1385.

- (6) Mounet, N.; Gibertini, M.; Schwaller, P.; Campi, D.; Merkys, A.; Marrazzo, A.; Sohier, T.; Castelli, I. E.; Cepellotti, A.; Pizzi, G.; Marzari, N. Two-dimensional Materials from High-throughput Computational Exfoliation of Experimentally Known Compounds. Nature nanotechnology 2018, 13, 246–252.
- (7) Zhang, X.; Zhang, Z.; Wu, D.; Zhang, X.; Zhao, X.; Zhou, Z. Computational Screening of 2D Materials and Rational Design of Heterojunctions for Water Splitting Photocatalysts. Small Methods 2018, 2, 1700359.
- (8) Paul, J.; Singh, A.; Dong, Z.; Zhuang, H.; Revard, B.; Rijal, B.; Ashton, M.; Linscheid, A.; Blonsky, M.; Gluhovic, D.; Guo, J.; Hennig, R. G. Computational Methods for 2D Materials: Discovery, Property Characterization, and Application Design. *Journal of Physics: Condensed Matter* 2017, 29, 473001.
- (9) Choudhary, K.; Kalish, I.; Beams, R.; Tavazza, F. High-throughput Identification and Characterization of Two-dimensional Materials Using Density Functional Theory. Scientific Reports 2017, 7, 1–16.
- (10) Haastrup, S.; Strange, M.; Pandey, M.; Deilmann, T.; Schmidt, P. S.; Hinsche, N. F.; Gjerding, M. N.; Torelli, D.; Larsen, P. M.; Riis-Jensen, A. C.; Gath, J.; Jacobsen, K. W.; Mortensen, J. J.; Olsen, T.; Thygesen, K. S. The Computational 2D Materials Database: High-throughput Modeling and Discovery of Atomically Thin Crystals. 2D Materials 2018, 5, 042002.
- (11) Zhou, J.; Shen, L.; Costa, M. D.; Persson, K. A.; Ong, S. P.; Huck, P.; Lu, Y.; Ma, X.; Chen, Y.; Tang, H.; Feng, Y. P. 2DMatPedia, an Open Computational Database of Two-dimensional Materials from Top-down and Bottom-up Approaches. *Scientific data* 2019, 6, 1–10.
- (12) Fronzi, M.; Ghazaleh, M. A.; Isayev, O.; Winkler, D. A.; Shapter, J.; Ford, M. J.

- Impressive Computational Acceleration by Using Machine Learning for 2-dimensional Super-lubricant Materials Discovery. arXiv preprint arXiv:1911.11559 2019,
- (13) Yang, T.; Zhou, J.; Song, T. T.; Shen, L.; Feng, Y. P.; Yang, M. High-Throughput Identifications of Exfoliable Two-Dimensional Materials with Active Basal Planes for Hydrogen Evolution. *ACS Energy Letters* **2020**,
- (14) Lu, S.; Zhou, Q.; Guo, Y.; Zhang, Y.; Wu, Y.; Wang, J. Coupling a Crystal Graph Multilayer Descriptor to Active Learning for Rapid Discovery of 2D Ferromagnetic Semiconductors/Half-Metals/Metals. Advanced Materials 2020, 2002658.
- (15) Kabiraj, A.; Kumar, M.; Mahapatra, S. High-throughput Discovery of High Curie Point Two-dimensional Ferromagnetic Materials. *npj Computational Materials* **2020**, *6*, 1–9.
- (16) Olsen, T.; Andersen, E.; Okugawa, T.; Torelli, D.; Deilmann, T.; Thygesen, K. S. Discovering Two-dimensional Topological Insulators from High-throughput Computations.

 Physical Review Materials 2019, 3, 024005.
- (17) Chen, A.; Zhang, X.; Zhou, Z. Machine Learning: Accelerating Materials Development for Energy Storage and Conversion. *InfoMat* **2020**, *2*, 553–576.
- (18) Zunger, A. Inverse Design in Search of Materials with Target Functionalities. *Nature Reviews Chemistry* **2018**, 2, 1–16.
- (19) Chen, Y.; Zhu, J.; Xie, Y.; Feng, N.; Liu, Q. H. Smart Inverse Design of Graphene-based Photonic Metamaterials by an Adaptive Artificial Neural Network. *Nanoscale* 2019, 11, 9749–9755.
- (20) Sorkun, M. C.; Astruc, S.; Koelman, J. V. A.; Er, S. An Artificial Intelligence-aided Virtual Screening Recipe for Two-dimensional Materials Discovery. npj Computational Materials 2020, 6, 1–10.

- (21) Dan, Y.; Zhao, Y.; Li, X.; Li, S.; Hu, M.; Hu, J. Generative Adversarial Networks (GAN) Based Efficient Sampling of Chemical Composition Space for Inverse Design of Inorganic Materials. npj Computational Materials 2020, 6, 1–7.
- (22) Goodfellow, I.; Pouget-Abadie, J.; Mirza, M.; Xu, B.; Warde-Farley, D.; Ozair, S.; Courville, A.; Bengio, Y. Generative Adversarial Nets. Advances in neural information processing systems. 2014; pp 2672–2680.
- (23) Arjovsky, M.; Chintala, S.; Bottou, L. Wasserstein Generative Adversarial Networks.

 International conference on machine learning. 2017; pp 214–223.
- (24) Davies, D. W.; Butler, K. T.; Jackson, A. J.; Skelton, J. M.; Morita, K.; Walsh, A. SMACT: Semiconducting Materials by Analogy and Chemical Theory. *Journal of Open Source Software* 2019, 4, 1361.
- (25) Butler, M.; Ginley, D. Prediction of Flatband Potentials at Semiconductor-electrolyte Interfaces from Atomic Electronegativities. *Journal of the Electrochemical Society* 1978, 125, 228.
- (26) Liaw, A.; Wiener, M. Classification and Regression by RandomForest. *R news* **2002**, *2*, 18–22.
- (27) Ward, L.; Agrawal, A.; Choudhary, A.; Wolverton, C. A General-purpose Machine Learning Framework for Predicting Properties of Inorganic Materials. *npj Computational Materials* **2016**, 2, 1–7.

(28)

- (29) Oganov, A. R.; Pickard, C. J.; Zhu, Q.; Needs, R. J. Structure Prediction Drives Materials Discovery. *Nature Reviews Materials* **2019**, *4*, 331–348.
- (30) Liang, H.; Stanev, V.; Kusne, A. G.; Takeuchi, I. CRYSPNet: Crystal Structure Predictions via Neural Network. arXiv preprint arXiv:2003.14328 2020,

- (31) Hargreaves, C. J.; Dyer, M. S.; Gaultois, M. W.; Kurlin, V. A.; Rosseinsky, M. J. The Earth Mover's Distance as a Metric for the Space of Inorganic Compositions. *Chemistry of Materials* **2020**,
- (32) Rubner, Y.; Tomasi, C.; Guibas, L. J. The Earth Mover's Distance as a Metric for Image Retrieval. *International journal of computer vision* **2000**, 40, 99–121.
- (33) Kresse, G.; Hafner, J. ab initio. Phys. Rev. B 1993, 47, 558–561.
- (34) Kresse, G.; Hafner, J. ab initio. Phys. Rev. B 1994, 49, 14251–14269.
- (35) G. Kresse, J. F. Efficiency of ab initio Total Energy Calculations for Metals and Semiconductors Using a Plane-Wave Basis Set. *Comput. Mater. Sci.* **1996**, *6*, 15–50.
- (36) Kresse, G.; Furthmüller, J. Efficient Iterative Schemes for ab initio Total-Energy Calculations Using a Plane-Wave Basis Set. *Phys. Rev. B* **1996**, *54*, 11169–11186.
- (37) Blöchl, P. E. Projector Augmented-Wave Method. Phys. Rev. B 1994, 50, 17953–17979.
- (38) Kresse, G.; Joubert, D. From Ultrasoft Pseudopotentials to the Projector Augmented-Wave Method. *Phys. Rev. B* **1999**, *59*, 1758–1775.
- (39) Perdew, J. P.; Burke, K.; Ernzerhof, M. Generalized Gradient Approximation Made Simple. *Phys. Rev. Lett.* **1996**, *77*, 3865–3868.
- (40) Perdew, J. P.; Burke, K.; Ernzerhof, M. Generalized Gradient Approximation Made Simple [Phys. Rev. Lett. 77, 3865 (1996)]. *Phys. Rev. Lett.* 1997, 78, 1396–1396.
- (41) Grimme, S.; Antony, J.; Ehrlich, S.; Krieg, H. A Consistent and Accurate ab initio Parametrization of Density Functional Dispersion correction (DFT-D) for the 94 elements H-Pu. The Journal of Chemical Physics 2010, 132, 154104.

- (42) Grimme, S.; Ehrlich, S.; Goerigk, L. Effect of the Damping Function in Dispersion Corrected Density Functional Theory. *Journal of Computational Chemistry* 32, 1456–1465.
- (43) Maaten, L. v. d.; Hinton, G. Visualizing Data using T-SNE. *Journal of machine learning research* **2008**, *9*, 2579–2605.
- (44) Goodall, R. E.; Lee, A. A. Predicting Materials Properties without Crystal Sructure: Deep Representation Learning from Stoichiometry. arXiv preprint arXiv:1910.00617 2019,
- (45) Baroni, S.; de Gironcoli, S.; Dal Corso, A.; Giannozzi, P. Phonons and Related Crystal Properties from Density-functional Perturbation Theory. Rev. Mod. Phys. **2001**, 73, 515–562.
- (46) Togo, A.; Tanaka, I. First Principles Phonon Calculations in Materials Science. Scr. Mater. 2015, 108, 1–5.
- (47) Jain, A.; Ong, S. P.; Hautier, G.; Chen, W.; Richards, W. D.; Dacek, S.; Cholia, S.; Gunter, D.; Skinner, D.; Ceder, G.; Persson, K. a. The Materials Project: A Materials Genome Approach to Accelerating Materials Innovation. *APL Materials* **2013**, *1*, 011002.
- (48) Hill, R. The Elastic Behaviour of a Crystalline Aggregate. *Proceedings of the Physical Society. Section A* **1952**, *65*, 349–354.
- (49) Mouhat, F.; Coudert, F.-X. Necessary and Sufficient Elastic Stability Conditions in Various Crystal Systems. *Physical Review B* **2014**, *90*.
- (50) Wang, V.; Xu, N.; Liu, J. C.; Tang, G.; Geng, W.-T. VASPKIT: a User-friendly Interface Facilitating High-throughput Computing and Analysis Using VASP Code. arXiv preprint arXiv:1908.08269 2019,